

Printable Hydraulics: A Method for Fabricating Robots by 3D Co-Printing Solids and Liquids

Robert MacCurdy¹, Robert Katzschmann¹, Youbin Kim¹, and Daniela Rus¹

Abstract—This work introduces a novel technique for fabricating functional robots using 3D printers. Simultaneously depositing photopolymers and a non-curing liquid allows complex, pre-filled fluidic channels to be fabricated. This new printing capability enables complex hydraulically actuated robots and robotic components to be automatically built, with no assembly required. The technique is showcased by printing linear bellows actuators, gear pumps, soft grippers and a hexapod robot, using a commercially-available 3D printer. We detail the steps required to modify the printer and describe the design constraints imposed by this new fabrication approach.

Index Terms—Additive Manufacturing, Flexible Robots, Soft Material Robotics, Printable Robotics, Hydraulic Robots.

I. INTRODUCTION

BUILDING robots has historically been a time-consuming process. Constrained by available fabrication techniques, conventional robotic design practice dictates that engineers sequentially assemble robots from many discrete parts, with long concomitant assembly times. Mass-production achieves efficiency gains through optimizing each assembly step, but optimization requires that the design be fixed; even small changes become difficult and costly. Additionally, because many robots are unique or application-specific, relatively few opportunities to automate their assembly exist. This situation is worsened by inevitable design-fabricate-test-redesign iterations.

Multi-material additive manufacturing techniques offer a compelling alternative fabrication approach, allowing materials with diverse mechanical properties to be placed at arbitrary locations within a structure, and enabling complex multi-part design iterations to be rapidly fabricated with trivial effort. In this work we present a new multi-material 3D printing process, *Printable Hydraulics*, capable of fabricating complete, functional, hydraulically actuated robotic structures in a single step. The key contribution of this work is a process that can simultaneously print solid and liquid materials.

Robots produced in this manner employ hydraulic channels to transmit force throughout the structure and incorporate large numbers of interconnected parts yet require no additional assembly steps, dramatically reducing fabrication time.

This work was supported by the National Science Foundation, grant numbers IIS-1226883 and CCF-1138967

¹Robert MacCurdy, Robert Katzschmann, Youbin Kim, and Daniela Rus are with the Computer Science and Artificial Intelligence Laboratory (CSAIL), MIT, 32 Vassar St, Cambridge, MA 02139, USA, {maccurdy, rkk, youbinkim, rus}@csail.mit.edu

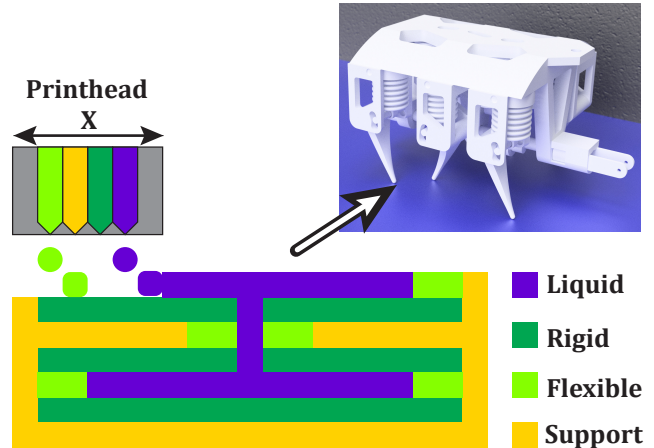


Fig. 1. Printable Hydraulics Fabrication via Inkjet: A 3D printer simultaneously deposits solid and liquid regions within a printed assembly. Prescribed strain in response to applied fluid pressure can be achieved either by printing with solids that have different elastic moduli or by designing appropriate model geometries. Supporting layers are provided via removable support material or liquid. As an example, a hexapod robot can be printed in one step, requiring only a single DC motor. The motor pumps fluid through the robot’s body, causing the legs to move.

In this paper we contribute:

- A new process for simultaneously fabricating mechanisms with solid and liquid components
- A 3D printer implementation (including modifications to existing 3D printers) to support the process
- Design constraints when using this method
- Demonstrations of the application to robotics by designing and printing: rigid actuators, soft actuators, fluid pumps, a soft gripper and a complete hexapod robot. All designs are printed in a single step.

A. Additive Manufacturing

Conventional fabrication methods employ predefined tooling to cut, extrude, stamp, and roll materials into desired geometries. These methods can be thought of as a continuous trade-off between versatility and throughput. For example, a stamping press with a die customized for a particular part can rapidly produce many identical copies of that part, but slight design modifications to the part require costly and time-consuming changes to the die. In contrast, a CNC milling machine with interchangeable tools can easily accommodate design changes, but is slower than stamping, is constrained by the reachable space of its tooling, and cannot readily create parts with heterogeneous structure. Additive manufacturing tools (“3D printers”) exist at the extreme of this continuum. They are relatively slow, but are enormously

versatile. In a recent book on 3D printing, Lipson and Kurman [1] enumerate 10 key principles of 3D printing; we repeat several here to highlight the potential benefits that additive manufacturing could offer roboticists. First, because 3D printers can produce arbitrary geometries, individual components can be co-fabricated in-situ, eliminating most or all assembly steps. This transforms the design space: complexity becomes free, once the 3D printer has been purchased, because incremental increases in design complexity do not require increases in fabrication complexity. Similarly, 3D printing makes the incremental cost of variety very low, allowing components to be diversified and specialized in an individual robot or across a suite of robots. Additionally, 3D printing reduces fabrication lead-times to zero, removes requirements for operator skill, and frees designers from most constraints imposed by the reachable space of the machine tool.

Unfortunately, these principles are primarily aspirational at present; many improvements in printers and printing materials will be required to fully realize 3D printing's potential. However, additive manufacturing is increasingly being leveraged by roboticists to decrease the production times of individual parts, and it enables individual part geometries that would be impractical or impossible to fabricate via conventional subtractive methods.

B. Related Work

3D printers have been demonstrated with a variety of model materials, ranging from ice to nylon to cookie dough. However, non-solidifying materials have not been widely used. A related approach, employed by some commercially-available 3D printers, uses wax as a support material; the wax solidifies soon after deposition and is melted away in a post-processing purging step [2]. This step imposes constraints on the aspect ratio of embedded channels and the channel termination, because long narrow channels, closed channels, or channels with large volumes at the end are difficult to purge. Other 3D printing systems employ a variety of solidifying support materials and have been used to fabricate microfluidic channels. However, like the wax support material, the solidified supporting material in these channels must be purged in a post-processing step. For this reason most 3D printed microfluidic applications are either planar [3], [4], or utilize small, easily cleaned sections requiring assembly [5]. When printing individual components that will be cleaned and then manually assembled, support materials that solidify are viable. On the other hand, this type of support is not suitable for fabricating complete hydraulically actuated assemblies.

Recently, 3D printing has been used to produce assembled, articulated and functional models, incorporating many (un-actuated) degrees of freedom [6], as well as entire kinematic chains for actuated models via interconnected gears and linkages [7], [8]. While this is an enabling capability for roboticists, printed gears and linkages currently suffer from high friction (since printed bearings have not been demonstrated), low-strength, low-resolution (which limits the

number of force-transmitting elements that can be placed in a given volume) and large backlash. Pneumatic systems overcome some of these backlash and friction challenges, but these structures have thus-far been produced in multiple assembly steps and require support material to be manually purged before inflating with the working gas [9], [10]. The use of compressible gas as the working fluid also creates force-density and control challenges. Other 3D-printed manipulators employ cable-driven linkages [11], which require several manual assembly steps.

II. PRINTABLE HYDRAULICS PROCESS

We define printed hydraulic parts as functional, hydraulically actuated assemblies that employ non-solidifying liquids as an active, permanent, force-transmitting component. These parts are printed in a single step, requiring no assembly. The schematic example in Fig. 1 shows the printed hydraulics concept applied to a 4-material inkjet printer. Such a printer can simultaneously fabricate solid and liquid regions within a structure. A print-head deposits individual droplets of material in a layer-by-layer build process. Each successive layer is deposited on the previous, and supports subsequent layers. Individual layers contain one or more material types, depending on the part geometry. Small droplet sizes (a 20-30 μm diameter is typical [12]), enable finely spaced patterns of the constituent materials to be deposited. The use of solids with varying stiffness allows certain portions to be more flexible, enabling prescribed strain in response to applied fluid pressure. Supporting layers are provided either via removable curing support material or by non-curing liquid.

While we focus primarily on inkjet deposition in this paper, the printable hydraulics approach can also be applied to other 3D printing methods. For example, stereolithography [13], [14] uses focused light to selectively solidify photopolymers in a layer-by-layer process. Rather than allowing the uncured material to drain out of the model, certain regions of liquid could be permanently enclosed. Similarly, 3D printers based on fused deposition molding (FDM) are now capable of depositing a variety of materials, including liquids, through interchangeable toolheads [15]. A dedicated nozzle with liquid could allow these multi-material FDM printers to create and then fill enclosed volumes with working fluid.

Printable hydraulics offers several benefits to designers of robots:

- No additional assembly is required because the force-transmitting fluid is deposited at the same time as the robot's solid body. This feature will enable complex actuated structures that would be inconvenient or impossible to assemble manually.
- Printed hydraulics enables complex, intricate geometries that are infeasible with other 3D printing methods. For example, removing support material from tortuous capillary-like structures is often impossible. This is the case even when using wax support when the aspect ratio of the channels is high, or when it is not possible to include purging ports in the design.

- Precise geometric control allows the creation of channels with differing resistances to fluid flow that can selectively distribute dynamic hydraulic flows to regions of the assembly. By varying the geometry and material composition of the cured (solid) regions of the assembly, graded elasticity can be achieved. Used together, these techniques can enable prescribed movements in response to changes in pressure from a single source, allowing under-actuated control through model geometry.
- The use of an incompressible working fluid simplifies the control of complex hydraulic assemblies, relative to systems based on pneumatics.
- There is no need to purge air bubbles because the solid and fluid regions are fabricated together.
- Non-curing liquids are useful as an easily-removed support structure for subsequent layers; this approach is widely used in the examples we show.
- Compared to previous work employing kinematic linkages or gears in active 3D printed assemblies, printed hydraulics offers low-friction, low-backlash, high force-transmission.

III. ARCHITECTING A 3D PRINTER FOR HYDRAULICS

The printer used in this work, a Stratasys Objet260 Connex, uses an inkjet head to deposit three different photopolymers simultaneously and achieves finished-part resolutions better than $100\mu\text{m}$. The Objet260 uses eight print-heads with linear arrays of nozzles to deposit resins onto the build surface. These resins rapidly cure when exposed to the high-intensity UV light source mounted on the print head. Three-dimensional models are broken up into thin slices, and printed from the bottom-up, layer by layer. The printer uses four heads for removable support (Objet printers use a soft, UV-cured solid for support) and allocates the remaining four heads to one or two model materials. Resins for the printer are supplied in plastic cartridges and these cartridges are labeled with an RFID chip, used by the printer to identify the material.

A. Printer Configuration

Stratasys sells a non-photopolymerizing material, composed primarily of polyethylene glycol according to the material safety datasheet, as a “model cleaning fluid”. This material is appropriate as a working hydraulic fluid, because it is designed to be jetted by the printheads, yet does not cure when exposed to UV light. The printer will not accept cleaning fluid as a working material, but the system can be spoofed by replacing the RFID chip in the cleaning fluid cartridge with one from a different model material; we chose an RFID chip from the Tango Black Plus material. This choice matters because the printer’s drive software, Objet Studio, automatically inserts several supporting layers underneath the model as it is being printed. Objet Studio will attempt to print the very first layers, the “carpet”, with a hard model material, if available. Choosing a softer material like Tango Black Plus as the spoofed type avoids depositing

two layers of non-curing liquid, which would not provide adequate support for successive layers above.

The Objet260 has two model material slots, labeled “Model 1” and “Model 2”. Objet Studio automatically intersperses model material within the automatically generated support material in order to stiffen the supporting structure; this inserted material is known as the “grid”. Inserting the liquid cartridge, which the printer recognizes as Tango Black Plus, into model slot two avoids printing liquid material as the grid (note that this is true for most, but not all model materials).

Inkjet printers deposit droplets of ink by applying a pulse of voltage to piezoelectric actuators located at each nozzle; the rapidly expanding piezo material displaces ink, forcing it through the nozzle. The nozzles’ driving waveforms are calibrated to the ink rheology. Although the inkjet nozzles can very precisely deposit droplets of ink, the precise height of each droplet is difficult to control. Even very small deviations in droplet volume could accumulate over many layers, resulting in printed layer heights substantially different from the CAD model. The Objet printers appear to address this issue by slightly over-driving the ink, and removing excess model material with a rotating drum, the “roller”, to provide a uniform layer height. As a side-effect, however, the roller tends to push uncured liquid in the direction of the head’s travel, forcing liquid to move out of its intended region, contaminating adjacent curing layers.

Objet Studio does not expose the nozzle drive waveform to the user, however it does allow the nozzle drive voltage to be calibrated - per head. When the cartridge containing liquid is loaded into model slot two, the liquid is routed to model heads M2 and M3. We determined experimentally that a head drive voltage of 19.4V delivered the best performance. Reducing the drive voltage of the liquid print-heads intentionally under-jets that material, resulting in less liquid in the model and lowering the level of liquid layers, relative to solid layers. This approach is an imperfect compromise, and imposes design constraints, discussed in section III-B.

B. Design Rules

Designing solid and liquid printed geometries follows many of the same steps as a conventional CAD/3D-printing work-flow. The liquid parts, like the solid parts, must be specified via an interchange file (STL is a commonly used format) and a model material in the printer is assigned to that file. In the case of the printed liquid, the spoofed material type (Tango Black Plus) should be assigned to the file specifying the liquid geometry. Note that all references to direction are with respect to the printer’s coordinate system, rather than the coordinate system of the part.

The Objet260 datasheet specifies an X/Y accuracy in the range of $20\text{--}85\mu\text{m}$, and a Z accuracy of $30\mu\text{m}$ when printing with multiple materials. However, we observed that the resolution at liquid-solid interfaces when printing liquids is substantially coarser. We characterized the achievable print resolution when printing with liquids by creating various test geometries and printing many iterations of these geometries

TABLE I

DESIGN RULES WHEN PRINTING WITH CURING AND NON-CURING MATERIALS USING A STRATASYS OBJET260 CONNEX 3D PRINTER. X IS ALIGNED ALONG PRINT-HEAD SCAN AXIS, Z IS PERPENDICULAR TO BUILD TRAY, Y FOLLOWS THE RIGHT-HAND-RULE

1	Separation (minimum along X/Y-axis):	0.4 mm
2	Separation (minimum along Z-axis):	0.2 mm
3	Feature thickness (minimum along X/Y-axis):	0.325 mm
4	Feature thickness (minimum along Z-axis):	0.2 mm
5	Feature growth (perpendicular to Y/Z-axis)	0.150 mm
6	Feature growth (perpendicular to X-axis)	0.2 mm
7	Solid-solid clearance at rotational joint	0.3 mm
8	Solid-over-liquid support thickness	0.2 mm
9	Solid-next-to-liquid support thickness	0.5 mm
10	Largest segment of liquid (dist in X or Y)	20 mm
11	Recommended width of support “pillars” inserted to connect model layers otherwise isolated by liquid; see Fig. 8 (X/Y-axis):	0.5 mm
12	Recommended solid feature thickness when adjacent to largest liquid segment (X/Y-axis):	2.11 mm

with different orientations on the build tray. These tests revealed the primary challenge when printing with liquids: non-curing materials are moved by the roller and swept onto adjacent curing regions. The presence of the non-curing material inhibits the bonding between droplets of solidifying material within the current layer, and between subsequent layers. This effect is most pronounced at solid/liquid boundaries perpendicular to the print-head’s direction of travel (interfaces parallel to the Y axis), and is exacerbated by long unbroken segments of liquid.

The clearances listed in Table I summarize our experimental observations and we refer to them by line number. Different solid features must be separated by at least $400\ \mu\text{m}$ of liquid in X/Y or $200\ \mu\text{m}$ in Z to remain distinct (lines 1 & 2). Solid features adjacent to liquid must be at least $325\ \mu\text{m}$ thick in X/Y or $200\ \mu\text{m}$ in Z to remain intact (lines 3 & 4). We also observed that features finish larger than designed. This is the case whether or not liquids are being printed, and the typical value is $150\ \mu\text{m}$ normal to the surface; however, when printing with liquids this value increases to $200\ \mu\text{m}$ for surfaces perpendicular (or nearly perpendicular) to the X axis (lines 5 & 6). Printed rotational joints are a key component of printed robots, but adequate clearance must be provided to ensure that adjacent solids do not fuse while minimizing backlash; we found $300\ \mu\text{m}$ to be an adequate trade-off (line 7). We discovered that introducing a thin shell of support material (by creating voids in the model geometries) that separates the solid from the liquid regions improves build-quality. This layer can be as thin as $200\ \mu\text{m}$ when the layer is nearly perpendicular to the Z axis, but should be at least $500\ \mu\text{m}$ when nearly parallel to the Z axis (lines 8 & 9). Finally, large contiguous regions of liquid in any particular layer should not exceed 20 mm (line 10), achieved by changing the model geometry or inserting $500\ \mu\text{m}$ diameter support “pillars” (line 11). These support pillars are also employed to anchor a new layer of solid when printed on top of a liquid layer. Solid features adjacent to large liquid regions should be as thick



Fig. 2. 3D-printed bellows produced via inkjet in a single print. Co-deposition of liquids and solids allows fine internal channels to be fabricated and pre-filled. The part is ready to use when it is removed from the printer.

as possible, particularly in the X direction. For example, our bellows design (Fig. 3) uses 2.11 mm thick solid regions on the layer that contains a 20 mm diameter circle of liquid (line 12).

Designs that adhere to these guidelines should be printable with good results, but apparently minor dimensional changes can have large impacts on the print quality. The most common failure mode occurs when unbonded cured material is swept up by the roller and deposited in the roller bath, clogging the drain that removes liquid. When this occurs, cured and uncured print material will often be deposited haphazardly over the build area, necessitating cleaning. It is critical that users become familiar with cleaning the roller bath assembly, the waste area, and the model heads before each print to ensure that the printer is clean and ready to print.

IV. FABRICATING ROBOTS

In the following we describe the design and use of bellows actuators as basic force transfer elements for printing hydraulic robots, and showcase their use in a hexapod robot. We also demonstrate a 3D printed fluid gear pump and explore the use of rubber-like materials by printing fluid-actuated soft grippers.

A. Bellows Actuator

A U-shaped bellows actuator is an axisymmetric shell convolution, consisting of many pleats in series; each pleat is a combination of two cut toroidal shells. These U-shaped

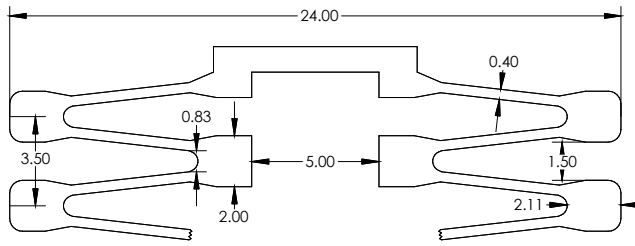


Fig. 3. Schematic design of a unit-section of the printed bellows; dimensions in mm. Additional displacement can be achieved by stacking multiple sections together.

bellows, also called expansion joints or compensators, are commonly made of metal and are used as compensating elements for thermal expansion and relative movement in pipelines, containers and machines. Fig. 2 shows the bellows actuator designed for this work.

Bellows actuators are more suitable for printed applications than pistons because the latter require sealing tolerances that are difficult to achieve with current 3D printers. Linear actuators based on a rolling diaphragm [16] also exhibit low-friction, and because they do not require sliding seals for expansion and contraction, they would be ideal for a 3D-printed part. Unfortunately, currently available printable photopolymers are not capable of sustaining the high material strains and withstanding the cyclic fatigue required by this design. While we preclude their use for now, we anticipate that new polymers will be released for commercially available printers, making printed linear actuators based on rolling diaphragms feasible.

Traditionally, bellows were made of a uniform thickness metal foil. The allowable thickness of this foil depends on several factors, including the working pressure, the desired bellows deformation and the allowable stress in the foil. However, the design rules described in Table I imply that a design with a uniform cross-section would need to be so thick that it would be excessively stiff. In response, we designed a bellows with a varying cross-sectional thickness (Fig. 3).

The varying cross-sectional thickness of our design necessitated an approach based on FEA to optimize the design geometry and anticipate the mechanical behavior of the printed part. Though a closed-form solution would require lower computational effort, there are limitations to finding closed-form solutions [17] for the stress analysis of bellows structures. The simplifications and assumptions required for closed-form solutions are described in [18] and [19]. These limitations motivate most bellows designers to use finite element analysis (FEA) methods [20]. Fig. 4 shows the result of FEA modeling a 2mm compression of the bellows actuator. We employed FEA using a range of Young's modulus values (900-1200 MPa). This range, which was informed by our compression test results, is lower than the manufacturer's stated range (1700-2100 MPa) for the photopolymer we used: Rigur (RGD450) from Stratasys. One possible explanation is that the material undergoes plastic deformation earlier in the strain cycle than we expect. Nevertheless, FEA analysis using a linear model is a useful tool for

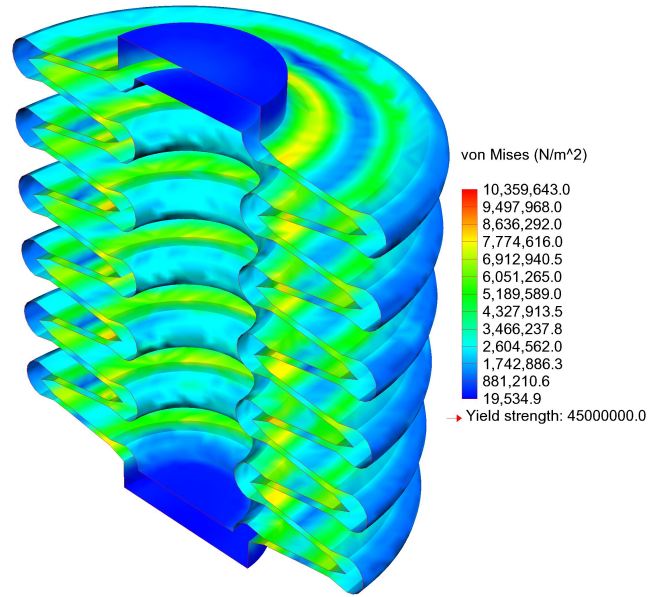


Fig. 4. Von-Mises-stress-analysis result of a cross section of one bellows. FEA allows design optimization via homogenization to mitigate stress concentrations.

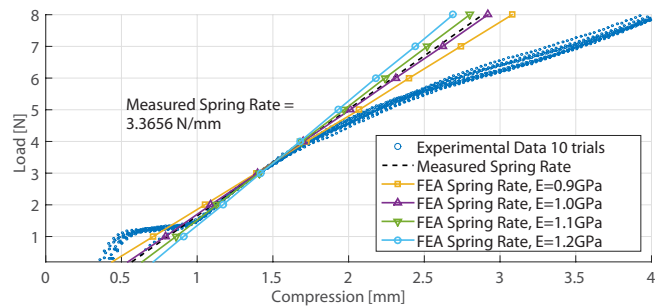


Fig. 5. Bellows compression experiments with no applied fluid pressure (port is open to the atmosphere) compared to finite element analysis experiments using 4 levels of young's modulus values. These tests reveal the intrinsic stiffness of this particular actuator design.

identifying stress concentrations in the part. The geometries of regions that exhibit excessive stress are modified using an iterative homogenization approach in order to reduce stress concentrations [21], while also adhering to the design guidelines that we experimentally determined and list in Table I.

Compression tests performed on an Instron 5944 mechanical loading platform allowed us to characterize the composite stiffness of the bellows design. The results of these compression tests, as well as the effective spring rates determined via FEA, are shown in Fig. 5. We measured the spring rate of several printed bellows that were open and had no fluid in them; 3-4 N/mm is typical of our designs. This number is significant from a system design viewpoint, since the fluid pressure driving the bellows must overcome the intrinsic stiffness of the bellows before it can do work on external loads.

A separate set of measurements show the actual force developed when fluid pressure is applied to a bellows actuator that is allowed to move in response to varying pressure. The

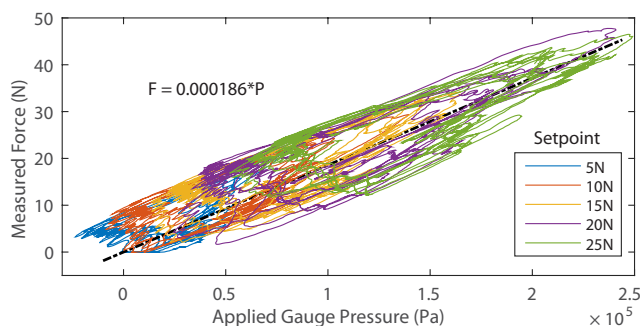


Fig. 6. Force developed vs. applied pressure for the bellows actuator shown. Tests were carried out at 5 operating force set points, and the actuator was allowed to extend and contract as a cyclic pressure activation was applied. The actuator exhibits hysteresis, likely due to friction at the rotary joints, visible as deviations from the linear trend line.

results of these measurements, shown in Fig. 6, reveal that a hysteresis loop is formed as the bellows is pressure-cycled. A least-squares fit of the pressure vs. force data yield a trend line with a slope of 186 mm^2 , which is the effective cross-sectional area of the bellows actuator if the bellows were modeled as a piston. This number is 60% of the actual internal area of the bellows cap (Fig. 3).

B. Hexapod Robot

To demonstrate the utility of the printed bellows design in an actual robot, we designed a tripod-gait hexapod with six rotational degrees of freedom (DOF), illustrated in Figs. 1 and 7. With the exception of the DC motor and power supply, all components of this robot are printed in a single step with no assembly required. This robot weighs 690 g, is 14 cm long, 9 cm wide and 7 cm tall. The legs are designed with a neutral position that inclines their major axis 60 degrees above the floor and each leg is actuated by a bellows, causing the leg to rotate 10 degrees in either direction, relative to this neutral position. Three of the legs are inclined toward the front of the robot (bank A) and three are inclined toward the rear (bank B).

Each driven bellows is internally connected to a corresponding driving bellows via a fluid channel that runs through the robot's body; the fluid in each driving/driven bellows pair is isolated from the other bellows. The three driving bellows from bank A are kinematically linked and attached to a crankshaft via a connecting rod. The bellows from bank B are similarly connected to a separate section of the crankshaft that is 90° out of phase. The crankshaft is turned at 30 RPM by a single geared DC motor consuming approximately 2 W (Pololu #3070), yielding a locomotion speed of 0.125 body-lengths per second. This arrangement moves the legs from the two banks 90° out of phase with each other, enabling forward or backward locomotion without an additional DOF at each leg, and does not require the feet to slide on the floor. The multimedia attachment illustrates this gait.

C. Gear Pump

Gear pumps are low-flow, high-pressure devices, are commonly employed in hydraulic systems and are capable of

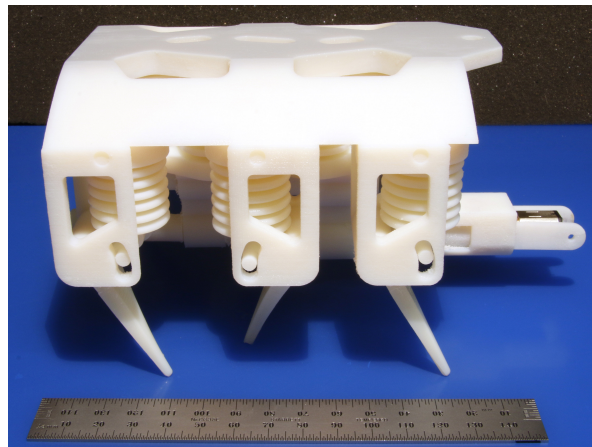


Fig. 7. The printed hexapod uses a tripod gait; a single DC motor spins a central crankshaft that pumps fluid via banks of bellows pumps directly above the crankshaft. Fluid is forced out of the pumps and distributed to each leg actuator by pipes embedded within the robot's body.

producing continuous flow. We designed and printed a gear pump to present an alternative to the bellows pump, which produces only reciprocating flow. The general design approach for gear pumps is well known [22] and their internal pressure transients and performance have been described elsewhere [23]. These pumps employ a pair of enmeshed counter-rotating teeth enclosed in a tight-fitting housing. Fluid trapped between the teeth and the housing is moved from the low-pressure port to the high pressure port, and is prevented from moving back by the meshed teeth near the center of the pump.

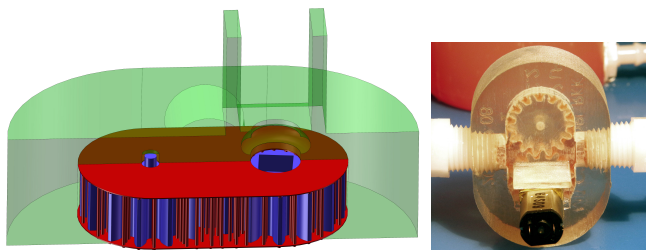


Fig. 8. 3D-printed gear pump realized via co-fabrication of solids and liquids in a single print. Gears are captive and fabricated in-place using liquid as support, allowing them to spin freely when powered by an added electrical motor. In the rendering, the pump housing is green, the gears are blue, and the support is red. Note the cylindrical support pillars (see Table I).

The section view of the pump prototype, Fig. 8, reveals the two meshed gears and their position within the housing. The gears have a pitch diameter of 17.5 mm, an outer diameter of 19.6 mm, a modulus of 1.25, and a gear height of 8 mm. We followed the common practice of using involute gears with a 20° pressure angle.

Like the bellows, the design of the gear pump was informed by the design rules listed in Table I. The gears are surrounded by a thin liquid layer that separates the gears from the housing's interior walls. The liquid clearance is $200 \mu\text{m}$. The pump design includes flat layers of rigid material that are directly above a layer of liquid, with no

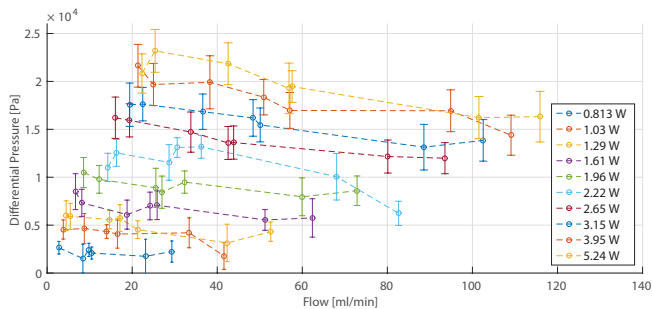


Fig. 9. Flow rate (ml/min) and pressure output through a variable load vs applied power (W) for the 3D-printed gear pump.

connection to another solid portion of the pump. This situation is problematic, leading to increased position uncertainty and the possibility that the roller will entirely remove new solid layers as they are deposited. The solution is to add arrays of small 500 μm diameter support pillars aligned along the Z axis that penetrate the liquid layer, providing an anchor for the new layer of solid while still being fragile enough to easily break down when the pump's gears are rotated. We also added thin 200 μm regions of support directly below solid layers that would otherwise rest on liquid. This improves the surface finish of the solid layer. Fig. 8 depicts these support regions in red, the gears in blue, and the housing in green. The liquid layer is not shown, but occupies the remaining negative space.

The pump performance was evaluated by measuring the pressure drop across a valve versus flow for different input power levels and valve positions [22]. The results are shown in Fig. 9. The test was performed using a small off-the-shelf brushed DC motor with a 250:1 gear ratio and a D-shaped output shaft that was inserted into one of the pump's gears.

D. Soft Gripper

The emerging field of Soft Robotics [24] offers a compelling alternative to traditional rigid-bodied robots, enabling structures that deform continuously [25], are robust [26], and are safer for human interaction [27]. Soft robots present the designer with a complex, continuous feature space; designers have employed modular design approaches [28] and evolutionary search to address this challenge [29], yielding body plans with complex geometries that are challenging to build with conventional methods. Soft robots also present unique actuation difficulties; embedded tensile elements (cables or SMA) [30], [31], and pneumatics [32], [26] are widely employed, though often at the cost of fabrication complexity.

Soft robots are usually fabricated via cast elastomers, and although casting soft robots is often faster than assembling conventional rigid robots, the mold-making process can be time consuming, and embedding multiple materials within a cast object via overmolding adds complexity. Additionally, producing complex, graded materials via casting is difficult. Additive manufacturing, combined with a printed hydraulics approach, provides an alternative fabrication method for soft robotics that is automated, flexible, and enables geometries that are infeasible with other production methods.

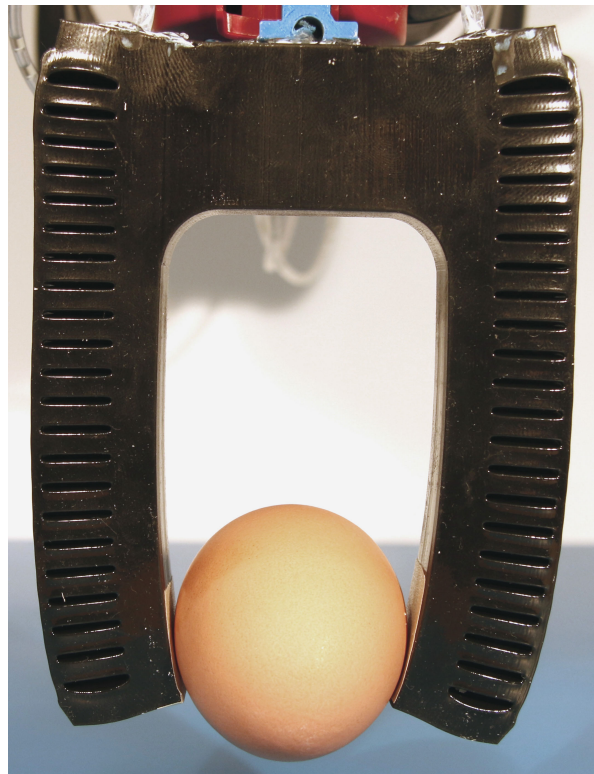


Fig. 10. 3D-printed soft gripper fabricated via inkjet deposition of a soft elastomer (28 Shore A) and a non-curing liquid (polyethylene glycol).

In [33] we used silicone rubber to cast a flexible gripper. As a demonstration of the utility of printable hydraulics to the soft robotics community, we designed and printed a similar two-finger soft gripper, shown in Fig. 10. The design process required six iterations. Each iteration required 3.5 hours to print and a short time to evaluate the performance of the part. This method is faster and requires less interaction than soft-robot fabrication approaches that rely on casting materials into molds. Additionally, the final gripper design incorporates thin channels and internal fluid routing that would be difficult to achieve via casting.

V. CONCLUSIONS

Building robots inevitably involves the time-consuming and labor-intensive step of assembling a large number of discrete pieces. 3D printers offer a way forward: by increasing the functionality of each part and fabricating ready-to-use assemblies of many parts, manual assembly steps can be reduced or eliminated. However, until now there has been no means of incorporating robust, high-performance force-transmission elements directly into a 3D-printed part. Our printed hydraulics method incorporates liquids into the designer's material palette, enabling embedded fluid-filled channels to be produced. This approach allows complex, functional, multi-part robotic assemblies that use hydraulic force transmission to be automatically fabricated. We demonstrated this method by printing a hexapod robot based on bellows actuators, a gear pump and a soft gripper.

Though we employed an inkjet printer for the current work, the concept of utilizing non-cured liquid as an active

component in a 3D printed assembly may also be applied to other 3D printing methods, including stereolithography and fused deposition modeling.

ACKNOWLEDGMENT

This work was funded in-part by an NSF grant: Expedition in Computing for Compiling Functional Physical Machines, # CCF-1138967. We are grateful for this support. The authors declare no competing financial interests. The authors would like to thank Victor Aladele for his help in developing the gear pump and Bianca Homberg for assistance in evaluating the gripper.

REFERENCES

- [1] H. Lipson and M. Kurman, *Fabricated: The New World of 3D Printing*, M. James, K. Kent, and D. Storti, Eds. John Wiley & Sons, 2013.
- [2] T. J. Snyder, M. Andrews, M. Weislogel, P. Moeck, J. Stone-Sundberg, D. Birkes, M. P. Hoffert, A. Lindeman, J. Morrill, O. Fercak *et al.*, “3d systems” technology overview and new applications in manufacturing, engineering, science, and education,” *3D Printing and Additive Manufacturing*, vol. 1, no. 3, pp. 169–176, 2014.
- [3] P. J. Kitson, M. H. Rosnes, V. Sans, V. Dragone, and L. Cronin, “Configurable 3d-printed millifluidic and microfluidic ‘lab on a chip’ reactionware devices,” *Lab on a Chip*, vol. 12, no. 18, pp. 3267–3271, 2012.
- [4] G. Comina, A. Suska, and D. Filippini, “Low cost lab-on-a-chip prototyping with a consumer grade 3d printer,” *Lab on a Chip*, vol. 14, no. 16, pp. 2978–2982, 2014.
- [5] K. C. Bhargava, B. Thompson, and N. Malmstadt, “Discrete elements for 3d microfluidics,” *Proceedings of the National Academy of Sciences*, vol. 111, no. 42, pp. 15013–15018, 2014.
- [6] J. Cali, D. A. Calian, C. Amati, R. Kleinberger, A. Steed, J. Kautz, and T. Weyrich, “3d-printing of non-assembly, articulated models,” *ACM Trans. Graph.*, vol. 31, no. 6, pp. 130:1–130:8, Nov. 2012. [Online]. Available: <http://doi.acm.org/10.1145/2366145.2366149>
- [7] B. Thomaszewski, S. Coros, D. Gauge, V. Megaro, E. Grinspun, and M. Gross, “Computational design of linkage-based characters,” *ACM Transactions on Graphics (TOG)*, vol. 33, no. 4, p. 64, 2014.
- [8] S. Coros, B. Thomaszewski, G. Noris, S. Sueda, M. Forberg, R. W. Sumner, W. Matusik, and B. Bickel, “Computational design of mechanical characters,” *ACM Transactions on Graphics (TOG)*, vol. 32, no. 4, p. 83, 2013.
- [9] D. B. Comber, J. E. Slightam, E. J. Barth, V. R. Gervasi, and R. J. Webster, “Design and precision control of an mr-compatible flexible fluidic actuator,” in *ASME/BATH 2013 Symposium on Fluid Power and Motion Control*. American Society of Mechanical Engineers, 2013, pp. V001T01A048–V001T01A048.
- [10] J. E. Slightam and V. R. Gervasi, “Novel integrated fluid-power actuators for functional end-use components and systems via selective laser sintering nylon 12,” in *23rd Ann Int Solid Freeform Fabrication Symp.* 2012, pp. 197–211.
- [11] A. Bruyas, F. Geiskopf, L. Meylheuc, and P. Renaud, “Combining multi-material rapid prototyping and pseudo-rigid body modeling for a new compliant mechanism,” in *Robotics and Automation (ICRA), 2014 IEEE International Conference on*. IEEE, 2014, pp. 3390–3396.
- [12] B. Derby, “Inkjet printing of functional and structural materials: fluid property requirements, feature stability, and resolution,” *Annual Review of Materials Research*, vol. 40, pp. 395–414, 2010.
- [13] C. W. Hull, “Apparatus for production of three-dimensional objects by stereolithography,” Mar. 11 1986, uS Patent 4,575,330.
- [14] J. R. Tumbleston, D. Shirvanyants, N. Ermoshkin, R. Januszewicz, A. R. Johnson, D. Kelly, K. Chen, R. Pinschmidt, J. P. Rolland, A. Ermoshkin, E. T. Samulski, and J. M. DeSimone, “Continuous liquid interface production of 3d objects,” *Science*, vol. 347, no. 6228, pp. 1349–1352, 2015. [Online]. Available: <http://www.sciencemag.org/content/347/6228/1349.abstract>
- [15] J. Lipton, R. MacCurdy, M. Boban, N. Chartrain, L. Withers III, N. Gangjee, A. Nagai, J. Cohen, K. S. J. Liu, H. Qudsi, J. Kaufman, and H. Lipson, “Fab@ home model 3: a more robust, cost effective and accessible open hardware fabrication platform,” in *Proceedings of the Twenty Third Annual International Solid Freeform Fabrication Symposium ? An Additive Manufacturing Conference, August 6-8, 2012, Austin, Texas, USA.*, 2012.
- [16] J. P. Whitney, M. F. Glisson, E. L. Brockmeyer, and J. K. Hodgins, “A low-friction passive fluid transmission and fluid-tendon soft actuator,” in *Intelligent Robots and Systems (IROS 2014), 2014 IEEE/RSJ International Conference on*. IEEE, 2014, pp. 2801–2808.
- [17] M. Tanaka, “Fatigue life estimation of bellows based on elastic-plastic calculations,” *International Journal of Pressure Vessels and Piping*, vol. 2, no. 1, pp. 51–68, 1974.
- [18] Y. Li and S. Sheng, “Strength analysis and structural optimization of U-shaped bellows,” *International Journal of Pressure Vessels and Piping*, vol. 42, no. 1, pp. 33–46, 1990.
- [19] P. Janzen, “Formulae and graphs of elastic stresses for design and analysis of U-shaped bellows,” *International Journal of Pressure Vessels and Piping*, vol. 7, no. 6, pp. 407–423, 1979.
- [20] H. Takatsu, M. Yamamoto, M. Shimizu, and M. Ohta, “Stress analysis method of U-shaped bellows and its experimental verification,” *Fusion Engineering and Design*, vol. 22, no. 3, pp. 239–250, 1993. [Online]. Available: <http://www.sciencedirect.com/science/article/pii/S0920379693901182>
- [21] M. P. Bendsøe and N. Kikuchi, “Generating optimal topologies in structural design using a homogenization method,” *Computer methods in applied mechanics and engineering*, vol. 71, no. 2, pp. 197–224, 1988.
- [22] I. J. Karassik, J. P. Messina, P. Cooper, and C. C. Heald, *Pump Handbook*. McGraw-Hill New York, 2008, vol. 4.
- [23] M. Eaton, P. S. Keogh, and K. A. Edge, “The modelling, prediction, and experimental evaluation of gear pump meshing pressures with particular reference to aero-engine fuel pumps,” *Proceedings of the Institution of Mechanical Engineers, Part I: Journal of Systems and Control Engineering*, vol. 220, no. 5, pp. 365–379, 2006. [Online]. Available: <http://dx.doi.org/10.1243/09596518jsce183>
- [24] H. Lipson, “Challenges and opportunities for design, simulation, and fabrication of soft robots,” *Soft Robotics*, vol. 1, no. 1, pp. 21–27, 2014.
- [25] C. Laschi, M. Cianchetti, B. Mazzolai, L. Margheri, M. Follador, and P. Dario, “Soft robot arm inspired by the octopus,” *Advanced Robotics*, vol. 26, no. 7, pp. 709 – 727, 2012.
- [26] M. T. Tolley, R. F. Shepherd, B. Mosadegh, K. C. Galloway, M. Wehner, M. Karpelson, R. J. Wood, and G. M. Whitesides, “A resilient, untethered soft robot,” *Soft Robotics*, vol. 1, no. 3, pp. 213–223, 2014.
- [27] A. Bicchi and G. Tonietti, “Fast and “soft-arm” tactics [robot arm design],” *Robotics Automation Magazine, IEEE*, vol. 11, no. 2, pp. 22–33, June 2004.
- [28] A. D. Marchese, R. K. Katzschmann, and D. Rus, “A recipe for soft fluidic elastomer robots,” *Soft Robotics*, vol. 2, no. 1, pp. 7–25, 2015.
- [29] N. Cheney, R. MacCurdy, J. Clune, and H. Lipson, “Unshackling evolution: Evolving soft robots with multiple materials and a powerful generative encoding,” in *Proceedings of the 15th annual conference on genetic and evolutionary computation (GECCO)*, 2013.
- [30] N. Cheng, M. Lobovsky, S. Keating, A. Setapen, K. Gero, A. Hosoi, and K. Iagnemma, “Design and analysis of a robust, low-cost, highly articulated manipulator enabled by jamming of granular media,” in *Robotics and Automation (ICRA), 2012 IEEE International Conference on*, May 2012, pp. 4328–4333.
- [31] H.-T. Lin, G. G. Leisk, and B. Trimmer, “Goqbot: a caterpillar-inspired soft-bodied rolling robot,” *Bioinspiration & biomimetics*, vol. 6, no. 2, p. 026007, 2011.
- [32] D. Rus and M. T. Tolley, “Design, fabrication and control of soft robots,” *Nature*, vol. 521, no. 7553, pp. 467–475, 2015.
- [33] R. K. Katzschmann, A. D. Marchese, and D. Rus, “Autonomous Object Manipulation using a Soft Planar Grasping Manipulator,” *Under Review: Soft Robotics*, 2015.